Resonant scattering of ^{22}Na + p studied by the thick-target inverse-kinematic method

S. J. Jin,[1] Y. B. Wang,[1,*] J. Su,[1] S. Q. Yan,[1] Y. J. Li,[1] B. Guo,[1] Z. H. Li,[1] S. Zeng,[1] G. Lian,[1] X. X. Bai,[1] W. P. Liu,[1] H. Yamaguchi,[2] S. Kubono,[2,3,4] J. Hu,[2,3] D. Kahl,[2] H. S. Jung,[5,†] J. Y. Moon,[5] C. S. Lee,[5] T. Teranishi,[6] H. W. Wang,[7] H. Ishiyama,[8] N. Iwasa,[9] T. Komatsubara,[10] and B. A. Brown[11]

[1]*China Institute of Atomic Energy, P.O. Box 275(10), Beijing 102413, China*
[2]*Center for Nuclear Study (CNS), University of Tokyo, RIKEN Campus, 2-1 Hirosawa, Wako, Saitama 351-0198, Japan*
[3]*Institute of Modern Physics, Chinese Academy of Sciences, Lanzhou 730000, China*
[4]*RIKEN Nishina Center, RIKEN Campus, 2-1 Hirosawa, Wako, Saitama 351-0198, Japan*
[5]*Department of Physics, Chung-Ang University, Seoul 156-756, Republic of Korea*
[6]*Department of Physics, Kyushu University, 6-10-1 Hakozaki, Fukuoka 812-8581, Japan*
[7]*Shanghai Institute of Applied Physics, Chinese Academy of Sciences, Shanghai 201800, China*
[8]*High Energy Accelerator Research Organization (KEK), 1-1 Oho, Tsukuba, Ibaraki 305-0801, Japan*
[9]*Department of Physics, Tohoku University, Aoba, Sendai, Miyagi 980-8578, Japan*
[10]*Department of Physics, University of Tsukuba, Ibaraki 305-8571, Japan*
[11]*Department of Physics and Astronomy, and National Superconducting Cyclotron Laboratory, Michigan State University, East Lansing, Michigan 48824-1321, USA*

(Received 17 May 2013; revised manuscript received 25 July 2013; published 3 September 2013)

Background: In presolar low-density graphite grains, an extraordinarily large ^{22}Ne/^{20}Ne ratio or even nearly pure ^{22}Ne is found, pointing to the condensation of radioactive ^{22}Na in grains. Supernovae and neon-rich novae are the main events that produce ^{22}Na via the explosive hydrogen burning process. The ^{22}Na$(p,\gamma)^{23}$Mg reaction is one of the key reactions that influences the ^{22}Na abundance in ejecta.

Purpose: The present work aims to explore the proton resonant states in ^{23}Mg relevant to the astrophysical ^{22}Na$(p,\gamma)^{23}$Mg reaction. The determined ^{23}Mg resonant parameters can be used to evaluate the ^{22}Na$(p,\gamma)^{23}$Mg reaction rate.

Method:A low-energy ^{22}Na radioactive ion beam is produced via the ^{1}H(^{22}Ne, ^{22}Na)n reaction, and used to measure the experimental excitation function of the ^{22}Na + p resonant scattering with a conventional thick-target inverse kinematic method. R-matrix analysis is applied to deduce the ^{23}Mg resonance parameters from the experimental excitation function.

Results: Three proton resonance states in ^{23}Mg are observed. Spins/parities and the proton partial widths are determined. The deduced excitation energies agree with the compiled values.

Conclusions: The new spin and parity assignments allow us to perform a shell-model calculation of the γ widths of the ^{23}Mg resonant states for the evaluation of the ^{22}Na$(p,\gamma)^{23}$Mg astrophysical reaction rate. The two s-wave resonant states established in this work at 8.793 and 8.916 MeV in ^{23}Mg, respectively, increase the total reaction rate by about 5% at a temperature greater than 2 GK.

DOI: 10.1103/PhysRevC.88.035801 PACS number(s): 25.60.−t, 25.40.Cm, 26.50.+x, 27.30.+t

I. INTRODUCTION

In 1972 Black found that in Orgueuil meteorites the abundance ratio of ^{20}Ne/^{22}Ne is less than 1.5, which is much smaller than that of 9.8 on earth; this is the so-called Ne-extraordinary (Ne-E) problem [1]. With the discovery and isolation of presolar grains from carbonaceous chondrites, it was soon realized that the highly enriched ^{22}Ne component carried by low-density graphite grains is dominantly from the extinct radioactivity of ^{22}Na [2,3]. In 1974, Clayton and Hoyle first suggested that the delayed 1.275 MeV γ ray from the decay of ^{22}Na may be used for the diagnosis of nova and supernova outbursts [4]. In the past 20 years, several observations with satellite-borne detectors have been attempted to verify the 1.275 MeV γ-ray emission from nearby novae. For example, the COMPTEL measurements of five recent Ne-type novae led to an upper limit of $3.7 \times 10^{-8} M_{\odot}$ of ^{22}Na ejected by any nova in the galactic disk [5].

The stellar sources of radioactive ^{22}Na are primarily created in neon-rich nova [6–9] and supernova explosions [10–12]. In neon-rich novae, ^{22}Na is produced via the sequence of reactions ^{20}Ne$(p,\gamma)^{21}$Na$(\beta^{+})^{21}$Ne$(p,\gamma)^{22}$Na, or ^{20}Ne$(p,\gamma)^{21}$Na$(p,\gamma)^{22}$Mg$(\beta^{+})^{22}$Na alternatively [3,6]. In core-collapse supernovae, ^{22}Na is mainly produced in the O/Ne zone by the ^{21}Ne$(p,\gamma)^{22}$Na reaction, where ^{21}Ne is produced by the ^{20}Ne$(n,\gamma)^{21}$Ne reaction and protons by ^{12}C(^{12}C, p)^{23}Na [10] or by the burst of neutrinos from the core [13]. Currently, mixing of matter from different supernova zones is necessary to explain the isotopic features of low-density graphite grains with core-collapse supernova signature [10,11,14]. In both nova and supernova scenarios, while the decay of ^{22}Na is delayed by its $T_{1/2} = 2.6$ y half-life, the ^{22}Na$(p,\gamma)^{23}$Mg

*Corresponding author: ybwang@ciae.ac.cn
†Present address: Department of Physics, University of Notre Dame, Notre Dame, Indiana 46556.

reaction rate over a large range of temperatures is crucial in deriving ranges of ^{22}Na production during nova and supernova outbursts.

Many experimental investigations have been carried out to reduce the uncertainties of the ^{22}Na$(p,\gamma)^{23}$Mg reaction rate. Direct measurements with radioactive ^{22}Na targets were performed by several groups [15–18], in which absolute or relative resonance strengths were obtained. Moreover, the complicated level structure of the odd-mass ^{23}Mg also attracted many spectroscopic studies by transfer reactions, for example ^{25}Mg$(p,t)^{23}$Mg [19], ^{24}Mg$(p,d)^{23}$Mg [20], and ^{22}Na$(^3$He$,d)^{23}$Mg [21], and by the β^+ decay of ^{23}Al [22–25], as well as by the heavy-ion fusion evaporation reaction ^{12}C$(^{12}$C$,n\gamma)^{23}$Mg [26,27]. In these studies new levels were identified in the energy region of astrophysical interest; however, most of the spectroscopic information and resonant properties are still missing for the ^{23}Mg levels above the proton threshold [28]. In this regard, the ^{22}Na $+$ p entrance channel plus resonant scattering with the thick-target inverse kinematics method [29] is sensitive to populate the relevant resonances in ^{23}Mg. In this work, we study proton resonant states in ^{23}Mg by using the ^{22}Na $+$ p resonant scattering, with a setup similar to our recent ^{26}Si $+$ p measurement [30]. The ^{22}Na$(p,\gamma)^{23}$Mg reaction rate is reevaluated by using both presently available and our new experimental data.

We first describe the experimental setup in Sec. II followed by the experimental results and R-matrix analysis in Sec. III. Our shell-model calculation is presented subsequently in Sec. IV, and the level properties comparing the experimental and theoretical results are discussed in Sec. V. Finally, the effect on the ^{22}Na$(p,\gamma)^{23}$Mg astrophysical reaction rate is presented in Sec. VI.

II. EXPERIMENT

A. Production of the ^{22}Na secondary beam

The experiment was carried out at the CNS (Center for Nuclear Study) radioactive ion beam separator (CRIB) [31,32] of the University of Tokyo located in the RIKEN radioactive ion beam factory (RIBF). CRIB is a low-energy, in-flight separator which receives beams from the RIKEN AVF cyclotron. By making use of charge-exchange or transfer reactions, CRIB can deliver intense, low-energy secondary beams for low- and medium-mass nuclei. Most of the produced radioactive ion beams have been used for resonant scattering experiments via the thick-target method [30,33–38], as is adopted in the present work.

In the present experiment, a ^{22}Na beam was produced via the ^{1}H$(^{22}$Ne, ^{22}Na$)n$ charge exchange reaction. The primary beam was ^{22}Ne^{7+} with an energy of 6.0 A MeV and an intensity of about 70 p nA delivered to CRIB. The hydrogen gas target for the production of ^{22}Na was confined in an 80 mm long cell by two Havar window foils, which were each 2.5 μm in thickness. The hydrogen gas was kept at a pressure of 400 ± 3 Torr and cooled with liquid nitrogen to a temperature of about 90 K [39], resulting in an effective thickness of 1.15 mg/cm^2. The ^{22}Na^{11+} particles were separated by magnetic rigidity at the momentum-dispersive focal plane and

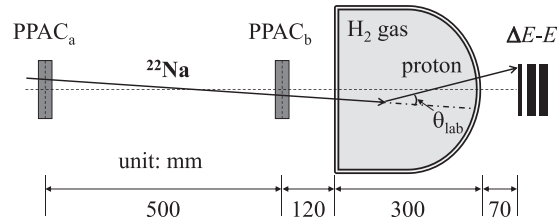

FIG. 1. Schematic layout of the experimental setup for the ^{22}Na $+$ p resonant scattering.

then focused into a spot of about 10–20 mm (FWHM) in diameter at the achromatic focal plane. The ^{22}Na beam was further purified by the Wien filter section. A nearly pure ^{22}Na beam was produced with an intensity of about 2.5×10^5 pps; the contaminant was mainly scattered ^{22}Ne^{10+} ions with a fraction of less than 7%.

B. ^{22}Na $+$ p measurement

A schematic layout of the experimental setup for the ^{22}Na $+$ p resonant scattering is shown in Fig. 1. The ^{22}Na beam particles were monitored by two parallel-plate avalanche counters (PPACs) before reaching the secondary hydrogen gas target. The timing and position information from the PPACs was used to determine the spatial velocity vector of the incoming particles on an event-by-event basis. The spatial resolution of the PPACs is about 1 mm [40]. The secondary gas target is semicylindrical in shape with a length of 300 mm. Its entrance window was 30 mm in diameter and sealed with a 2.5 μm Havar foil, while the exit window was also 30 mm in height and sealed with a 26.5 μm aluminized Mylar foil. The energy of the ^{22}Na secondary beam after the entrance window of the gas target was 37.1 ± 1.0 MeV, which was measured with a calibrated single-pad silicon detector (SD) in the ^{22}Na beam tuning runs; during these runs, the secondary gas target was removed from the beamline, and an SD partly covered by a 2.5 μm Havar foil was inserted. During the ^{22}Na $+$ p measurement, the hydrogen gas target was maintained within 310 ± 2 Torr by a gas-flow system; this pressure was chosen to fully stop the ^{22}Na particles in the gas volume.

The lighter recoil particles emerging from the exit window were detected by a silicon-detector telescope (ST) centered at $\theta_{lab} = 0^\circ$. The ST consists of ΔE and E layers, where the ΔE layer is a double-sided silicon strip detector (DSSD) with orthogonally oriented 16×16 readout strips on both sides and the E layer is an SD. One additional SD was used to veto any energetic light ions produced in the production target and satisfying the $B\rho$ selection, possibly not rejected entirely by the Wien filter because of scattering in the inner wall of the beamline or some other reasons. All three silicon detectors have an area of 50 mm $\times$ 50 mm. The thickness of the ΔE detector is 75 μm and that of the E detectors is about 1.5 mm. Recoil protons were identified by using the ΔE-E scatter plot and the time-of-flight information. The proton energy was deduced from the sum of ΔE and E, and the corresponding silicon detectors were calibrated using proton beams from CRIB and using standard α sources of ^{237}Np,

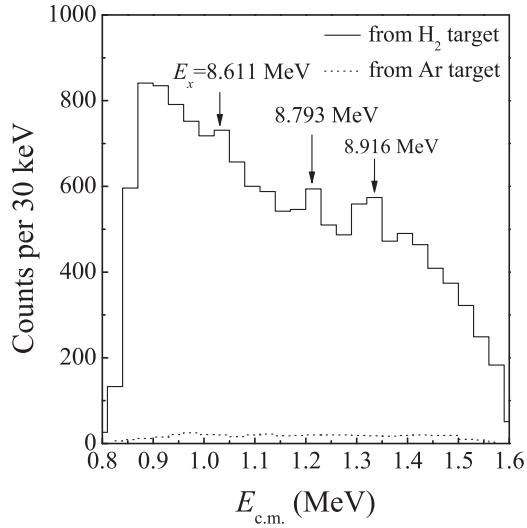

FIG. 2. Proton yields of the ^{22}Na + p resonant elastic scattering. A bin size of 30 keV is chosen based on the evaluated experimental $E_{c.m.}$ uncertainty. See text for details.

^{241}Am, and ^{244}Cm. The recoil particle spectrum with argon gas of equivalent stopping power was also measured separately to evaluate the background proton events originating from any source other than from the hydrogen gas.

III. RESULTS

A. Experimental results

By taking the two-body kinematics of ^{1}H(^{22}Na, p)^{22}Na elastic scattering and by considering the energy losses of ^{22}Na and proton along their trajectories, the $E_{c.m.}$ was deduced from the kinematic reconstruction on an event-by-event basis; although the actual measurement was performed in inverse kinematics, throughout the rest of the text we will denote it as ^{22}Na(p, p) for simplicity. At a laboratory angle θ_{lab}, the center-of-mass energy $E_{c.m.}$ has a simple relation with the proton energy E_p,

$$E_{c.m.} = \frac{M_b + M_p}{4M_b \cos^2\theta_{lab}} E_p, \tag{1}$$

where E_p is the energy of the recoil proton at the reaction point, M_b and M_p are the masses of the ^{22}Na beam and the proton, respectively, and θ_{lab} is the laboratory scattering angle of the emitted proton relative to the ^{22}Na beam-particle direction. The energy resolution of $E_{c.m.}$ was determined by the resolution of the silicon ΔE-E detectors, the resolution of θ_{lab}, the energy spread of the ^{22}Na beam, and the particle straggling in the target and foil materials. Monte Carlo simulations that include these components were performed, and the evaluated $E_{c.m.}$ uncertainty was about $\pm$20 to $\pm$15 keV according to increasing $E_{c.m.}$.

Proton yield of the ^{22}Na(p, p) resonant scattering at $\theta_{c.m.} = 180^\circ$ is shown in Fig. 2 together with the proton background obtained with argon gas. The proton background spectrum is flat, and after normalization to the total number of incident ^{22}Na beam ions comprises merely 2% of the number of protons seen in the main run with the hydrogen target. The net proton yield is then obtained by subtracting the normalized proton background events. The laboratory averaged differential cross section for the ^{22}Na + p elastic scattering is deduced from the net proton yield according to [41]

$$\left(\frac{d\sigma}{d\Omega}\right)_{lab} = \frac{\frac{dN_p}{dE}}{I_{beam}\frac{dN_t}{dE}d\Omega}, \tag{2}$$

where dN_p/dE refers to the net proton yield per $E_{c.m.}$ unit, dN_t/dE is the energy dependent number of hydrogen atoms, I_{beam} is the total number of incident ^{22}Na particles, and $d\Omega$ is the solid angle.

In the experimental geometry, the ST covers a different range of scattering angles depending on the depth in the gas target. Only proton events with $\theta_{lab} \leqslant 5^\circ$ were selected in the calculation of the experimental differential cross section. The necessary corrections of the effective area of the silicon telescope were made correspondingly for $d\Omega$ of each $E_{c.m.}$ bin.

B. *R*-matrix analysis

The averaged differential cross section in the center-of-mass frame is obtained by

$$\left(\frac{d\sigma}{d\Omega}\right)_{c.m.} = \frac{1}{4\cos\theta_0}\left(\frac{d\sigma}{d\Omega}\right)_{lab}, \tag{3}$$

where θ_0 is the averaged laboratory scattering angle of 0°. The excitation function of the ^{22}Na(p, p) elastic scattering is shown in Fig. 3. The uncertainties of the differential cross section include the statistical and systematic errors; the latter one is from the uncertainties in determining the solid angle and the effective number of target atoms.

The experimental excitation function has been analyzed by using a new-edition R-matrix code [42], which enables multichannel multilevel R-matrix fitting calculation of the excitation function taking the experimental $E_{c.m.}$ resolution into account. The R-matrix element $R_{c'c}$ takes the form of

$$R_{c'c} = \sum_{\lambda} \frac{\gamma_{\lambda c'}\gamma_{\lambda c}}{E_\lambda - E}, \tag{4}$$

where the subscripts c and c' denote different channels and λ the level index [43]. The reduced width $\gamma^2_{\lambda c}$ is related to the Coulomb penetration probability $P(l)$ by

$$\gamma^2_{\lambda c} = \Gamma_{\lambda c}/2P(l), \tag{5}$$

where $\Gamma_{\lambda c}$ is the particle width. The $P(l)$ is defined by

$$P(l) = kr/\left(F_l^2 + G_l^2\right)\big|_{r_c}, \tag{6}$$

where k is the wave number, and F_l and G_l are the regular and irregular Coulomb wave functions for a given relative orbital angular momentum l. The channel radius is given by $r_c = r_0(A_t^{1/3} + A_p^{1/3})$, where A_t and A_p are the mass numbers of the target and projectile, respectively. The R-matrix fitting calculation is not very sensitive to changes of r_0 in the 1.2 to 1.6 fm range, so a standard value of $r_0 = 1.25$ fm is taken in the calculation shown in Fig. 3.

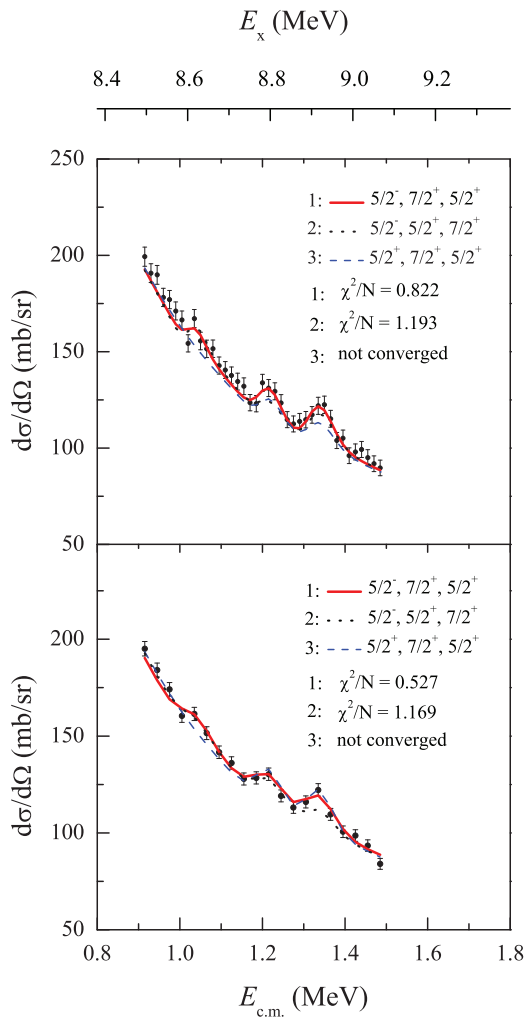

FIG. 3. (Color online) Excitation function of the ^{22}Na(p, p) elastic scattering shown in two different bin sizes of 15 keV (upper panel) and 30 keV (lower panel). The best R-matrix fits including three resonances with $J^\pi = (5/2 \text{ to } 9/2)^-$, $7/2^+$, and $5/2^+$, respectively, are shown with solid lines. The deduced resonant parameters are consistent with the two different bin sizes. The dotted and dashed lines show the fitting results with different spin and parity assignments for comparison.

The spin and parity of the ground state of ^{22}Na is 3^+, there are thus two possible channel spins of $5/2^+$ and $7/2^+$, respectively, for the ^{22}Na + p elastic channel. The largest orbital angular momentum is 1 for the measured $E_{\text{c.m.}}$ range, therefore only $l = 0$, 1 need to be considered in the R-matrix analysis. Three peaks have been seen at $E_R = 1.030$, 1.212, and 1.335 MeV in the excitation function. The corresponding excitation energy of ^{23}Mg is $E_x = E_R + S_p$, where the ^{23}Mg proton separation energy is $S_p = 7.581$ MeV according to the latest mass measurements of ^{22}Na [44] and ^{23}Mg [45] with Penning-trap mass spectrometers. Since the γ widths of the resonances are negligible compared to the particle widths, only the proton decay channel to the ground state of ^{22}Na is taken into account in the fitting calculation. The best R-matrix fit to the excitation function includes three resonances with $J^\pi = (5/2 \text{ to } 9/2)^-$, $7/2^+$, and $5/2^+$, respectively. A negative parity is assigned to the 8.611 MeV state in ^{23}Mg definitively due to the signature of an $l = 1$ proton resonance; however, a spin value of 5/2 to 9/2 shows no noticeable difference in the results of the R-matrix analysis. The spin and parity for the 8.793 and 8.916 MeV ^{23}Mg states can be explicitly assigned with $7/2^+$ and $5/2^+$, respectively, according to the proton s-wave resonances. The resonance energies and proton partial widths of the observed ^{23}Mg states are also deduced from the R-matrix analysis, as listed in Table I.

IV. SHELL-MODEL CALCULATION

The explicit assignments of the spin and parity to the 8.793 and 8.916 MeV resonances in ^{23}Mg allow for the shell-model calculation of the proton spectroscopic factors and the γ widths. According to the method developed by Schiffer [46], the proton partial width Γ_p can be defined by the proton spectroscopic factor C^2S and Γ_{sp} as

$$\Gamma_p = C^2 S \, \Gamma_{sp}, \tag{7}$$

where Γ_{sp} denotes the single-particle proton decay width. We calculate Γ_{sp} by proton scattering on a Woods-Saxon potential.

The shell-model calculation for the $l = 0$ resonances in ^{23}Mg is performed with the NUSHELLX code [47] by using the method developed recently for astrophysical resonant reaction rates [48,49]. The calculations are performed in the sd-shell model space with USDA and USDB interactions [50] for the charge-independent part plus the Coulomb, charge-dependent, and charge-asymmetric nuclear Hamiltonian obtained by Ormand and Brown for the sd shell [51]. The calculated results for ^{23}Mg states from 8 to 9 MeV are listed in Table II. The proton spectroscopic factor C^2S refers to the proton $l = 0$ transitions to the $2s_{1/2}$ single-particle orbital in the $^{22}\text{Na}_{g.s.}$ + p final states.

V. DISCUSSION

The correspondence between the experimental and the shell-model calculated $5/2^+$,$7/2^+$ states in ^{23}Mg is shown in Fig. 4. The observed ^{23}Mg resonant states are listed in Table I along with the previous data for comparison.

A. 8.611 MeV state

We suggest a negative parity and a spin range of 5/2 to 9/2 for the 8.611 MeV excited state in ^{23}Mg according to the R-matrix analysis of the experimental excitation function. A level at 8.617 MeV is found in the data compilations [52,53], which were mainly based on the ^{25}Mg(p, t)^{23}Mg angular distribution measurement [19]. Although the excitation energies are almost the same, the level was suggested to be associated with an $l \geqslant 4$ transition [19].

A similar ^{23}Mg level at 8.617 MeV was observed in the ^{22}Na(p, γ)^{23}Mg reaction direct measurement, and an upper limit of the resonance strength was also predicted [15]. The low $E_{\text{c.m.}}$ energy of the resonance indicates its low-l transfer character, which turns to support the assignment of the present work.

TABLE I. The deduced resonant parameters from the experimental excitation function of ^{22}Na(p, p) along with the previous data for comparison. The resonant parameters are averaged values of the results from the excitation functions with the different bin sizes of 15 and 30 keV. The excitation energy E_x in ^{23}Mg is obtained by the sum of E_R and the ^{23}Mg proton separation energy $S_p = 7.581$ MeV.

This work			^{25}Mg(p, t)^{23}Mg[a]		^{22}Na(p, γ)[b]		^{23}Al decay	
E_x (MeV)	J^π	Γ_p^{expt} (keV)	E_x (MeV)	J^π	E_x (MeV)	$\omega\gamma$ (meV)	E_x (MeV)[c]	E_x (MeV)[d]
8.611(20)	(5/2 to 9/2)$^-$	3.2(1.0)	8.617(6)		8.617	$\leqslant$79		
8.793(13)	7/2$^+$	1.2(0.3)	8.793(8)		8.793	$\leqslant$69	8.785(8)	8.781(3)
8.916(15)	5/2$^+$	2.3(0.7)	8.916(6)	(3/2 to 13/2)$^+$			8.919(9)	8.905(3)

[a]Reference [19].
[b]Reference [15].
[c]Reference [24].
[d]Reference [25].

B. 8.793 MeV 7/2$^+$ state

The 8.793 MeV ^{23}Mg resonance was observed in the direct measurements with a radioactive ^{22}Na target [15], resulting in an upper limit of the resonance strength. The level was recently confirmed in the β-decay experiments as delayed proton lines [24,25]. The calculated single-particle width is 67 keV from this work, leading to an experimental spectroscopic factor of 0.023(4). The experimental energy and spectroscopic factor are in best agreement with the ninth theoretical 7/2$^+$ state in Table II. However, the experimental spectroscopic factor is about a factor of 3 larger than theory. For the astrophysical rate we use the experimental proton-decay width of 1.2(3) keV and the calculated gamma-decay width of 0.20(7) eV—an average of the USDA and USDB results with an error that is typical of the differences between USDA and USDB results. Since $\Gamma_p \gg \Gamma_\gamma$, the astrophysical reaction rate depends only on Γ_γ.

C. 8.916 MeV 5/2$^+$ state

An 8.916(6) MeV state in ^{23}Mg was observed in the ^{25}Mg(p, t)^{23}Mg angular distribution measurement [19] but assigned as an $l = 4$ transition. A level with similar energy of 8.905(3) MeV was identified in the recent β-decay experiment [25]. In the present work, an explicit spin-parity assignment of 5/2$^+$ can be made to the resonance based on the R-matrix analysis of the excitation function. The calculated single-particle width is 182 keV from this work, leading to an experimental spectroscopic factor of 0.014(5). The experimental energy and spectroscopic factor are in best agreement with the 12th theoretical 5/2$^+$ state in Table II. For the astrophysical rate we use the experimental proton-decay width of 2.3(7) keV and the calculated gamma decay with a width of 1.9(7) eV—the average of the USDA and USDB results, with an error that is typical of the differences between the USDA and USDB results. Since $\Gamma_p \gg \Gamma_\gamma$, the astrophysical reaction rate depends only on Γ_γ.

D. Inelastic scattering channel

In present work, no indication of the inelastic scattering is directly observed, therefore the resonance parameters are obtained by the assumption of only the ^{22}Na + p elastic scattering channel in the R-matrix analysis. The lowest three excited states in ^{22}Na are 1$^+$, 0$^+$, and 4$^+$ states at 583, 657, and 891 keV, respectively, which are at least energetically allowed to accommodate proton decay from the populated ^{23}Mg resonant states. However, the first two excited states in ^{22}Na allow for only proton d-wave transitions, which should be largely hindered by the low Coulomb penetration probabilities due to larger l value and smaller $E_{\text{c.m.}}^{\text{inel}}(p) = E_R - E_x(^{22}\text{Na})$.

Only the 891 keV ^{22}Na 4$^+$ state allows for a proton s-wave transition from the 8.793 MeV 7/2$^+$ resonance in

TABLE II. Shell-model calculation of the $l = 0$ resonances in ^{23}Mg above the proton separation energy. See text for details.

	USDA			USDB		
J^π	E_x (MeV)	C^2S	Γ_γ (eV)	E_x (MeV)	C^2S	Γ_γ (eV)
$5/2^+_9$	7.890	0.0000	1.88	7.860	0.0000	3.29
$5/2^+_{10}$	8.338	0.0340	1.50	8.421	0.0320	1.83
$5/2^+_{11}$	8.649	0.0054	1.01	8.615	0.0036	0.52
$5/2^+_{12}$	8.959	0.0170	1.94	8.991	0.0200	1.94
$5/2^+_{13}$	9.021	0.0003	1.73	9.471	0.0003	2.74
$7/2^+_8$	8.042	0.1050	0.26	7.911	0.1050	0.40
$7/2^+_9$	8.650	0.0077	0.27	8.423	0.0081	0.13
$7/2^+_{10}$	8.996	0.0058	1.43	9.055	0.0069	1.22
$7/2^+_{11}$	9.332	0.0134	1.65	9.249	0.0130	1.57

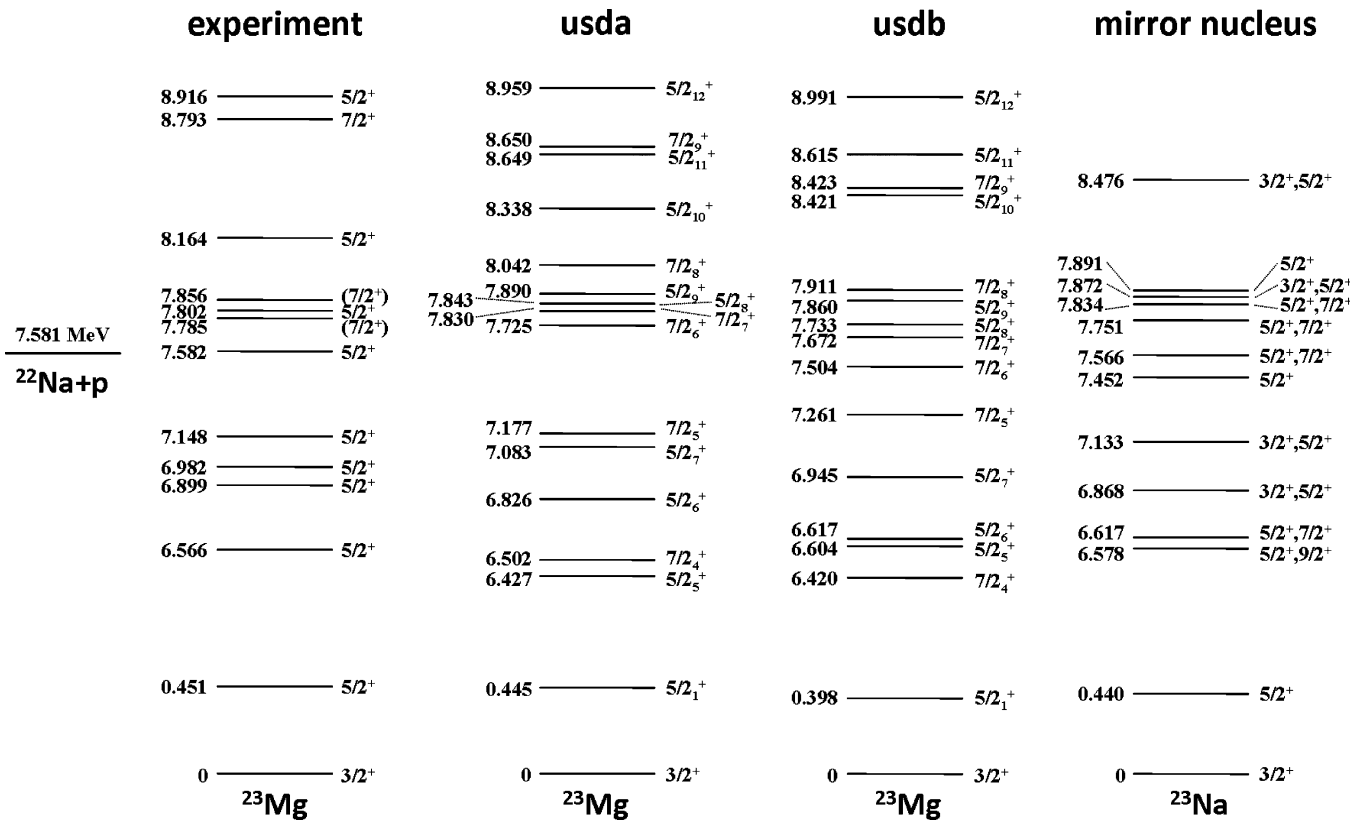

FIG. 4. The correspondence between the experimental and the shell-model calculated $5/2^+$, $7/2^+$ states in ^{23}Mg; the corresponding levels in the mirror nucleus ^{23}Na are also shown for comparison.

^{23}Mg. The calculated proton spectroscopic factor with USDB interaction is 0.0335 for the inelastic channel comparing to 0.0081 for the elastic channel. However, the Coulomb penetration probability would decrease by more than three orders of magnitude for the inelastic branch because of the small $E^{\rm inel}_{\rm c.m.}(p) = E_R - E_x(^{22}{\rm Na})$ of about 320 keV. Therefore, the proton partial width for inelastic scattering should be negligible according to Eq. (7). The β-delayed proton lines observed only to the ground state of ^{22}Na also support such an argument [24,25].

VI. ASTROPHYSICAL REACTION RATE

The ^{22}Na$(p,\gamma)^{23}$Mg astrophysical reaction rate can be evaluated, by combining the resonance parameters obtained in the present work for the 8.793 and 8.916 MeV states in ^{23}Mg and the shell-model calculated γ widths. The resonant reaction rate for isolated and narrow resonances is calculated as a sum over all relevant resonant states above the proton threshold [54,55]:

$$N_A\langle\sigma v\rangle_r = 1.540\times10^{11}(\mu T_9)^{-3/2} \times \sum_f \omega\gamma_{if} e^{-11.605E_R/T_9}\ {\rm cm^3 s^{-1} mol^{-1}}, \quad (8)$$

where N_A is the Avogadro constant, μ is the reduced mass in amu, T_9 is the dimensionless temperature defined by $T_9 = T/(10^9\ {\rm K})$, and E_R the resonance energy in MeV, respectively. The resonance strength $\omega\gamma$ (in MeV) is

$$\omega\gamma = \frac{2J_f+1}{(2J_i+1)(2J_p+1)}\frac{\Gamma_p\Gamma_\gamma}{\Gamma_p+\Gamma_\gamma}, \quad (9)$$

where J_i, J_p, and J_f are the spins of the target, the proton, and the resonant state in the compound ^{23}Mg, respectively. Since $\Gamma_p \gg \Gamma_\gamma$ in this case, the resonance strength becomes $\omega\gamma \simeq \omega\Gamma_\gamma$. The relevant parameters obtained in the present work used for the ^{22}Na$(p,\gamma)^{23}$Mg reaction rate calculation are listed in Table III.

The reaction rate of ^{22}Na$(p,\gamma)^{23}$Mg for the resonances observed in the present work is shown in Fig. 5. The compiled reaction rate [56] and the one from a recent direct measurement [18,57] are also shown for comparison. The two s-wave resonances established in this work increase the total reaction rate by about 5% at $T > 2$ GK, which is within the peak temperature of supernova outbursts.

TABLE III. Relevant parameters obtained in the present work used for the reaction rate calculation.

		USDA		USDB	
E_x (MeV)	J^π	Γ_γ (eV)	$\omega\gamma$ (eV)	Γ_γ (eV)	$\omega\gamma$ (eV)
8.793	$7/2^+$	0.27	0.16	0.13	0.07
8.916	$5/2^+$	1.94	0.83	1.94	0.83

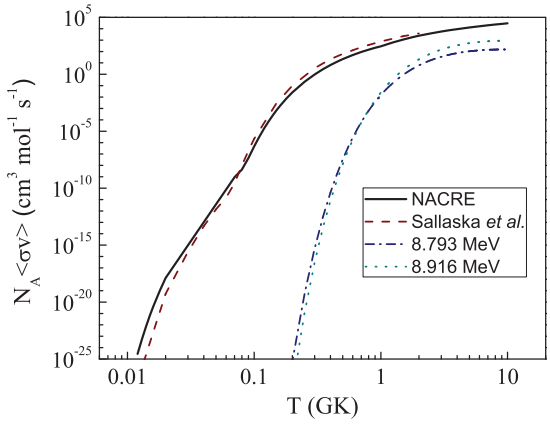

FIG. 5. (Color online) The reaction rate of ^{22}Na(p, γ)^{23}Mg for the resonances observed in the present work.

VII. SUMMARY

The ^{22}Na + p resonant scattering has been studied via the thick-target inverse kinematic method at the CRIB separator. The excitation function for ^{22}Na(p, p) was obtained and analyzed with the R-matrix fitting calculations. Three resonant states in ^{23}Mg have been observed, and the resonant parameters are determined. The explicit assignments of the spin and parity to the 8.793 and 8.916 MeV resonances in ^{23}Mg allow for the shell-model calculation of the proton spectroscopic factors and the γ widths, and consequently the evaluation of the resonant reaction rate. An enhancement of the total reaction rate on the order of 5% over the evaluation by NACRE is found for $T_9 > 2$ owing to the two s-wave resonant states established in this work. The present work showed that new and important spectroscopic information on the structure of ^{23}Mg relevant to the ^{22}Na(p, γ)^{23}Mg reaction rate can be obtained by using the ^{22}Na + p resonant scattering. Further similar measurements with a high-resolution active target are particularly necessary to reach the lower resonant energy region of the ^{22}Na(p, γ)^{23}Mg reaction.

ACKNOWLEDGMENTS

This work was performed at the RI Beam Factory operated by RIKEN Nishina Center and CNS, the University of Tokyo. We are grateful to the CNS and RIKEN accelerator staff for the smooth operation of the machine. We thank Professor Pierre Descouvemont of Université Libre de Bruxelles (ULB) for providing us with the R-matrix code and instructive communications. This work is supported by the National Natural Science Foundation of China under Grants No. 11021504, No. 11175261, No. 11105229 and the 973 Program of China under Grant No. 2013CB834406, as well as by the JSPS KAKENHI (No. 21340053) and the Priority Centers Research Program in Korea (No. 2009-0093817). BAB acknowledges support from NSF Grant No. PHY-1068217.

[1] D. C. Black, Geochim. Cosmochim. Acta **36**, 347 (1972).
[2] D. D. Clayton, Nature (London) **257**, 36 (1975).
[3] M. Arnould and H. Nørgaard, Astron. Astrophys. **64**, 195 (1978).
[4] D. D. Clayton and F. Hoyle, Astrophys. J. **187**, L101 (1974).
[5] A. F. Iyudin *et al.*, Astron. Astrophys. **300**, 422 (1995).
[6] J. José, A. Coc, and M. Hernanz, Astrophys. J. **520**, 347 (1999).
[7] S. Amari, X. Gao, L. R. Nittler, E. Zinner, J. José, M. Hernanz, and R. S. Lewis, Astrophys. J. **551**, 1065 (2001).
[8] C. Iliadis, A. Champagne, J. José, S. Starrfield, and P. Tupper, Astrophys. J. Suppl. Ser. **142**, 105 (2002).
[9] P. A. Denissenkov, J. W. Truran, M. Pignatari, R. Trappitsch, C. Ritter, F. Herwig, U. Battino, and K. Setoodehnia, arXiv:1303.6265 (2013).
[10] S. Amari, Astrophys. J. **690**, 1424 (2009).
[11] P. R. Heck, S. Amari, P. Hoppe, H. Baur, R. S. Lewis, and R. Wieler, Astrophys. J. **701**, 1415 (2009).
[12] M. M. M. Meier, P. R. Heck, S. Amari, H. Baur, and R. Wieler, Geochim. Cosmochim. Acta **76**, 147 (2012).
[13] D. Clayton, *Handbook of Isotopes in the Cosmos* (Cambridge University Press, Cambridge, 2003).
[14] T. Yoshida, Astrophys. J. **666**, 1048 (2007).
[15] J. Görres, M. Wiescher, S. Graff, R. B. Vogelaar, B. W. Filippone, C. A. Barnes, S. E. Kellogg, T. R. Wang, and B. A. Brown, Phys. Rev. C **39**, 8 (1989).
[16] S. Seuthe *et al.*, Nucl. Phys. A **514**, 471 (1990).
[17] F. Stegmüller, C. Rolfs, S. Schmidt, W. H. Schulte, H. P. Trautvetter, and R. W. Kavanagh, Nucl. Phys. A **601**, 168 (1996).
[18] A. L. Sallaska *et al.*, Phys. Rev. Lett. **105**, 152501 (2010).
[19] H. Nann, A. Saha, and B. H. Wildenthal, Phys. Rev. C **23**, 606 (1981).
[20] S. Kubono *et al.*, Z. Phys. A **348**, 59 (1994).
[21] S. Schmidt, C. Rolfs, W. H. Schulte, H. P. Trautvetter, R. W. Kavanagh, C. Hategan, S. Faber, B. D. Valnion, and G. Graw, Nucl. Phys. A **591**, 227 (1995).
[22] K. Peräjärvi, T. Siiskonen, A. Honkanen, P. Dendooven, A. Jokinen, P. O. Lipas, M. Oinonen, H. Penttilä, and J. Äystö, Phys. Lett. B **492**, 1 (2000).
[23] V. E. Iacob, Y. Zhai, T. Al-Abdullah, C. Fu, J. C. Hardy, N. Nica, H. I. Park, G. Tabacaru, L. Trache, and R. E. Tribble, Phys. Rev. C **74**, 045810 (2006).
[24] A. Saastamoinen *et al.*, Phys. Rev. C **83**, 045808 (2011).
[25] O. S. Kirsebom, H. O. U. Fynbo, A. Jokinen, M. Madurga, K. Riisager, A. Saastamoinen, O. Tengblad, and J. Äystö, Eur. Phys. J. A **47**, 130 (2011).
[26] D. G. Jenkins *et al.*, Phys. Rev. Lett. **92**, 031101 (2004).
[27] D. G. Jenkins *et al.*, Phys. Rev. C **87**, 064301 (2013).
[28] H. Comisel, C. Hategan, G. Graw, and H. H. Wolter, Phys. Rev. C **75**, 045807 (2007).
[29] K. P. Artemov *et al.*, Sov. J. Nucl. Phys. **52**, 408 (1990).
[30] H. S. Jung *et al.*, Phys. Rev. C **85**, 045802 (2012).
[31] S. Kubono *et al.*, Eur. Phys. J. A **13**, 217 (2002).
[32] Y. Yanagisawa *et al.*, Nucl. Instrum. Methods A **539**, 74 (2005).
[33] T. Teranishi *et al.*, Phys. Lett. B **556**, 27 (2003).
[34] T. Teranishi *et al.*, Phys. Lett. B **650**, 129 (2007).
[35] J. J. He *et al.*, Phys. Rev. C **76**, 055802 (2007).
[36] H. Yamaguchi *et al.*, Phys. Lett. B **672**, 230 (2009).
[37] J. J. He *et al.*, Phys. Rev. C **80**, 015801 (2009).
[38] H. Yamaguchi *et al.*, Phys. Rev. C **87**, 034303 (2013).

[39] H. Yamaguchi, Y. Wakabayashi, G. Amadio, S. Hayakawa, H. Fujikawa, S. Kubono, J. J. He, A. Kim, and D. N. Binh, Nucl. Instrum. Methods A **589**, 150 (2008).
[40] H. Kumagai, A. Ozawa, N. Fukuda, K. Sümmerer, and I.˜Tanihata, Nucl. Instrum. Methods A **470**, 562 (2001).
[41] S. Kubono, Nucl. Phys. A **693**, 221 (2001).
[42] P. Descouvemont and D. Baye, Rep. Prog. Phys. **73**, 036301 (2010).
[43] A. M. Lane and R. G. Thomas, Rev. Mod. Phys. **30**, 257 (1958).
[44] G. Savard *et al*., Phys. Rev. C **70**, 042501(R) (2004).
[45] A. Saastamoinen *et al*., Phys. Rev. C **80**, 044330 (2009).
[46] J. P. Schiffer, Nucl. Phys. **46**, 246 (1963).
[47] NuShellX@MSU, B. A. Brown, W. D. M. Rae, E. McDonald, and M. Horoi, http://www.nscl.msu.edu/∼brown/resources/resources.html; NuShellX, W. D. M. Rae, http://www.garsington.eclipse.co.uk/.
[48] W. A. Richter, B. A. Brown, A. Signoracci, and M. Wiescher, Phys. Rev. C **83**, 065803 (2011).
[49] W. A. Richter and B. A. Brown, Phys. Rev. C **85**, 045806 (2012).
[50] B. A. Brown and W. A. Richter, Phys. Rev. C **74**, 034315 (2006).
[51] W. E. Ormand and B. A. Brown, Nucl. Phys. A **491**, 1 (1989).
[52] P. M. Endt, Nucl. Phys. A **633**, 1 (1998).
[53] R. B. Firestone, Nucl. Data Sheets **108**, 1 (2007).
[54] W. A. Fowler and F. Hoyle, Astrophys. J. Suppl. **9**, 201 (1964).
[55] C. E. Rolfs and W. S. Rodney, *Cauldrons in the Cosmos* (The University of Chicago Press, Chicago, 1988).
[56] C. Angulo *et al*., Nucl. Phys. A **656**, 3 (1999).
[57] A. L. Sallaska *et al*., Phys. Rev. C **83**, 034611 (2011).